NANO LETTERS

2008
Vol. 8, No. 11
3904-3910

Determining the Internal Quantum Efficiency of PbSe Nanocrystal Solar Cells with the Aid of an Optical Model

Matt Law,*,† Matthew C. Beard,† Sukgeun Choi, Joseph M. Luther, Mark C. Hanna, and Arthur J. Nozik

National Renewable Energy Laboratory, Golden, Colorado 80401

Received August 2, 2008; Revised Manuscript Received September 5, 2008

ABSTRACT

We determine the internal quantum efficiency (IQE) of the active layer of PbSe nanocrystal (NC) back-contact Schottky solar cells by combining external quantum efficiency (EQE) and total reflectance measurements with an optical model of the device stack. The model is parametrized with the complex index of refraction of each layer in the stack as calculated from ellipsometry data. Good agreement between the experimental and modeled reflectance spectra permits a quantitative estimate of the fraction of incident light absorbed by the NC films at each wavelength, thereby yielding well-constrained QE spectra for photons absorbed only by the NCs. Using a series of devices fabricated from 5.1 ± 0.4 nm diameter PbSe NCs, we show that thin NC cells achieve an EQE and an active layer IQE as high as 60 ± 5% and 80 ± 7%, respectively, while the QE of devices with NC layers thicker than about 150 nm falls, particularly in the blue, because of progressively greater light absorption in the field-free region of the films and enhanced recombination overall. Our results demonstrate that interference effects must be taken into account in order to calculate accurate optical generation profiles and IQE spectra for these thin film solar cells. The mixed modeling/experimental approach described here is a rigorous and powerful way to determine if multiple exciton generation (MEG) photocurrent is collected by devices with EQE < 100%. On the basis of the magnitudes and shapes of the IQE spectra, we conclude that the 1,2-ethanedithiol treated NC devices studied here do not produce appreciable MEG photocurrent.

Light absorption in a thin film solar cell can be greatly affected by optical interference if the device is optically thin and has a highly reflective back electrode. When these conditions are met, the buildup of an optical mode structure will change the absorption spectra of the active materials relative to their spectra when free of the optical cavity formed by the device stack. Exponential, Beer's Law type absorption/generation profiles cannot then be assumed, and accurate values of the internal quantum efficiency (IQE) of the active layers of the device can be obtained only by determining their absorption spectra as they exist within the device structure.

The IQE of a solar cell is normally calculated from the ratio of its external quantum efficiency (EQE) and spectral absorptance as $\mathrm{IQE}(\lambda) = \mathrm{EQE}(\lambda)/[1 - \rho(\lambda) - \tau(\lambda)]$, where $\rho(\lambda)$ is the spectral reflectance and the device transmittance $\tau(\lambda)$ is usually zero. However, this approach can give an underestimated and misleading IQE spectrum if incident light is absorbed by the electrodes and other nonactive layers of the device in addition to the active semiconductor layer(s). We show here that the quantum efficiency of photons absorbed only within the active layer of a PbSe nanocrystal back-contact Schottky solar cell[1] can be determined by combining reflectance measurements with an optical model capable of discerning the fraction of light absorbed in each of the layers within the device stack. An accurate determination of the IQE is essential for ascertaining whether multiple exciton generation (MEG) photocurrent is generated by these devices. An IQE substantially greater than 100% for sufficiently high-energy photons ($h\nu \geq 3E_g$) would indicate that MEG is occurring.

Experimental Section. ***Materials.*** Lead oxide (PbO, 99.999%), selenium (99.99%), oleic acid (OA, tech. grade, 90%), diphenylphosphine (DPP, 98%), 1-octadecene (ODE, 90%), and anhydrous solvents were purchased from Aldrich and used as received. Trioctylphosphine (TOP, tech. grade, >90%) and 1,2-ethanedithiol (EDT, >98%) were acquired from Fluka. Calcium pieces (99.99%) and aluminum shot (99.999%) were purchased from Cerac and Aldrich, respectively.

NC Synthesis. A single 0.8 g sample of NCs having a first exciton transition at 1686 nm (0.735 eV) was used for this study. The NCs were synthesized and purified using standard airfree techniques. A solution of 3.01 g PbO (13.5 mmol), 10.61 g oleic acid (37.6 mmol), and 0.514 g DPP

* To whom correspondence should be addressed. Present address: Department of Chemistry, University of California, Irvine. E-mail: matt.law@uci.edu.

† These authors contributed equally to this work.

10.1021/nl802353x CCC: $40.75
Published on Web 09/30/2008

(2.76 mmol) in 70.05 g ODE was degassed and heated to 180 °C in a reaction flask for one hour. Thirty-five milliliters of a 1 M solution of TOP-Se was then rapidly injected into this hot solution. The NCs were grown at 145 °C for 90 s, and the reaction was rapidly quenched with a water bath and 50 mL of anhydrous hexane. The NCs were purified by precipitation twice in hexane/acetone and once in hexane/ethanol and stored in a glovebox as a powder.

Device Fabrication. PbSe NC films were deposited onto precleaned, patterned ITO-coated glass substrates (12 Ω/sq., Colorado Concept Coatings) using a layer-by-layer dip coating procedure modified from our previous reports[1,2] to yield uniform, optically perfect films across larger areas (square inches). Rather than dipping the films by hand, a mechanical dip coater mounted inside of a glovebox (DC-Multi-4, Nima Technology) repetitively dipped the substrates into a 4 mg mL^{-1} solution of NCs in dry hexane and then a 0.002 M solution of 1,2-ethanedithiol (EDT) in dry acetonitrile. Glassy, crack-free, and mildly conductive ($\sigma = 5 \times 10^{-5}$ S cm^{-1} in the dark) NC films are produced in this way. Film thickness is linear with the number of dipping cycles for a fixed dipping speed (Supporting Information, Figure S1). We fabricated NC films with thicknesses in the 30−450 nm range. Unwanted areas of each film were removed with a razor blade. Top contacts (15 nm Ca/60 nm Al) were then deposited through a shadow mask in a glovebox thermal evaporator (2×10^{-8} Torr base pressure, Angstrom Engineering) at a rate of 0.2 Å s^{-1} for the Ca and 1.0 Å s^{-1} for the Al. This procedure yields six devices per substrate, each with an active area of 0.105 cm^2.

Characterization, Modeling, and Device Testing. The complex refractive index $\tilde{n}(\lambda) = n(\lambda) + ik(\lambda)$ of the glass, ITO, NC film, and Al layers were determined from 200 to 1700 nm by rotating compensator-type, variable-angle spectroscopic ellipsometry (J. A. Woollam Co. M2000) at room temperature. The incidence angle was varied from 65 to 75° and the spectral resolution was 1.6 nm. Transmittance measurements were acquired in a normal-incidence configuration. Samples were prepared on undoped, polished silicon substrates or glass microscope slides and measured under a continuous flow of dry nitrogen seconds after removing them from airfree transfer tubes. The measured data were analyzed using the multiphase model (substrate/interface roughness/film/surface roughness/ambient). A set of Gaussian and Lorentzian oscillators was employed in the model to reproduce the optical spectra of the films. The thickness and surface roughness of each sample were also estimated by scanning electron microscopy (SEM) (JEOL JSM-700F) and atomic force microscopy (AFM) (Veeco Dimension 3100 in tapping mode). The film thicknesses and the surface roughnesses determined by ellipsometric measurements were in good agreement with the results from SEM and AFM analyses. We found the optical functions of the NC films to be independent of film thickness. The resulting $n(\lambda)$ and $k(\lambda)$ of each material were then used to parametrize the optical model of the device.

For reflectance measurements, large-area device stacks (6.5 cm^2) were prepared on unpatterned ITO-coated glass substrates that were dip coated alongside the patterned substrates used for devices. Total reflectance curves of the large-area stacks were acquired from 300−2200 nm using a Shimadzu UV-3600 spectrophotometer equipped with a 60 mm integrating sphere (8° incidence angle) and a NIST-calibrated specular reflectance standard (STAN-SSH, Ocean Optics). Transmission of light through the devices was negligible at all wavelengths.

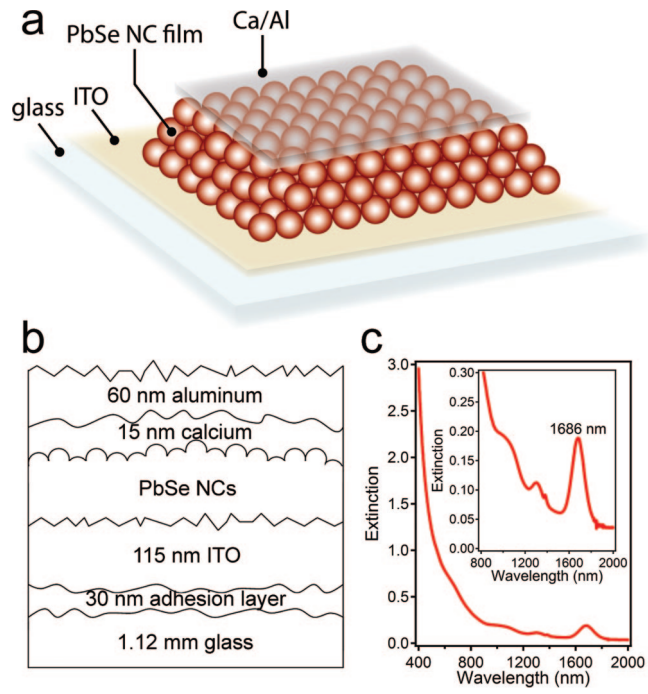

Figure 1. (a) A cartoon of the PbSe NC Schottky solar cell. Light is incident through the glass, and the charge-separating electric field is located at the NC/Ca interface. (b) The device stack in cross section, showing the thickness and schematic roughness of each layer. (c) An absorption spectrum of a solution of the 5.1 ± 0.4 nm diameter PbSe nanocrystals used in this study. The width of the first excitonic transition at 1686 nm is 51 meV.

Current−voltage and EQE measurements were performed in a glovebox without exposing the devices to air. An ELH-type tungsten halogen lamp set to 100 mW cm^{-2} with calibrated filtered Si diodes (Hamamatsu, S1787−04) served as the solar simulator. Photocurrents were not corrected for spectral mismatch between the ELH bulb and the true AM1.5G solar spectrum. EQE measurements were performed without bias illumination from 330−1750 nm in 10 nm steps with a fiber-coupled monochromator, a Stanford Research Systems SR830 lock-in amplifier (locked to light chopped at 153 Hz), and a calibrated silicon/germanium sandwich diode (Judson, J16SI-8A4-R03M-SC) for UV-NIR wavelengths. Masking the devices during the $I-V$ and EQE measurements did not affect the results.

Results and Discussion. The structure of the PbSe NC Schottky cell is shown in Figure 1. It is a sandwich of six distinct layers: a 1.12 mm thick float glass substrate, a 30 nm thick SiO_2 barrier layer, a 115 ± 5 nm thick ITO coating, a PbSe NC film of variable thickness, a 15 ± 4 nm thick calcium layer of significant roughness, and an opaque 60 nm thick aluminum electrode. The surface roughness of the glass, barrier layer, and ITO were determined by ellipsometry

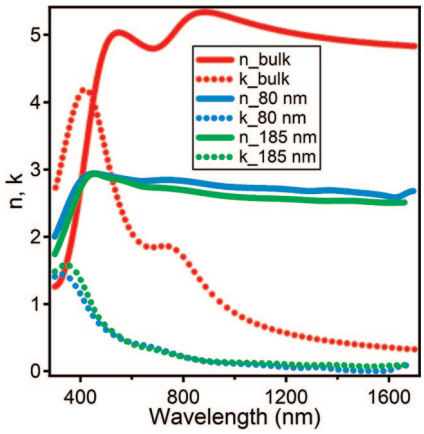

Figure 2. The optical constants of PbSe NC films of two different thicknesses (80 and 185 nm) relative to values for bulk PbSe (see ref 14). The NC data vary by less than 10% for 300−1000 nm, but $k(\lambda)$ shows substantial relative variation from 1100−1600 nm (difficult to see because of the small magnitude of $k(\lambda)$ in this region of the spectrum).

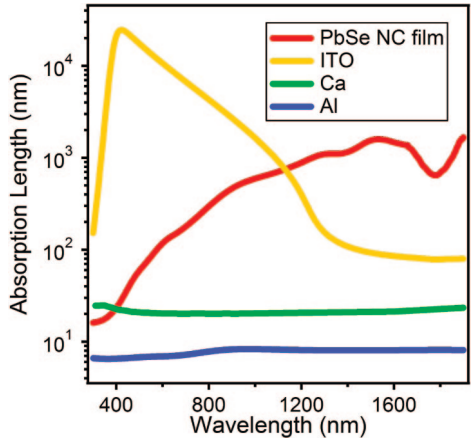

Figure 3. Optical penetration depths of the different layers in the device stack.

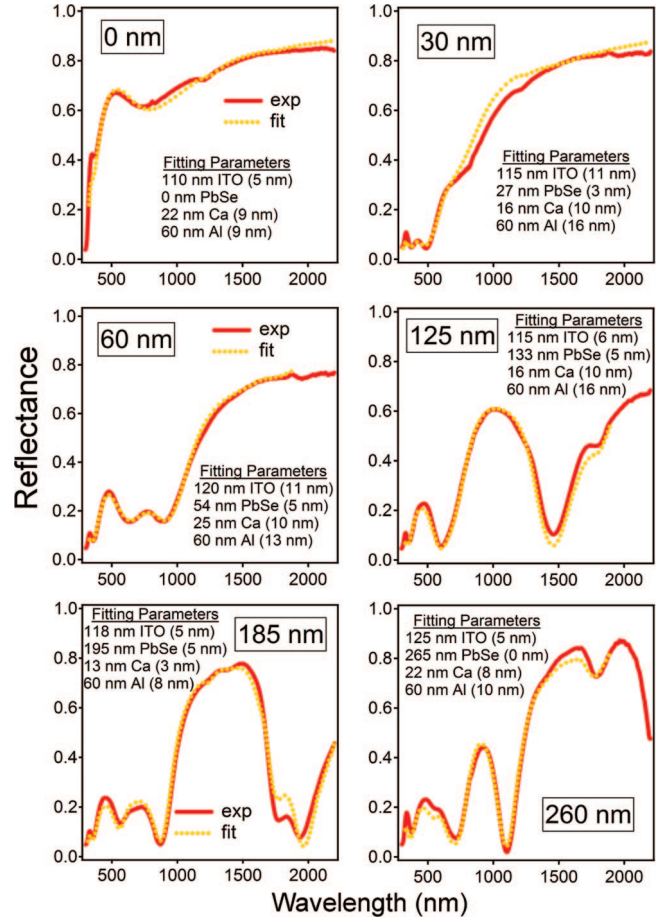

Figure 4. Experimental and modeled reflectance curves of devices with NC film thicknesses from 0 to 260 nm (as determined by AFM and SEM). The incidence angle is 8°. The thickness and roughness (in parentheses) of the layers found by each nonlinear least-squares fit are indicated. The fitting parameters were allowed to vary within the following limits: 110−125 nm ITO, 10−25 nm Ca, and 0−20 nm rms interfacial roughness. All fits employed a 1.12 mm thick glass substrate and 30 nm adhesion layer with 5 nm of roughness.

and AFM measurements to be 5−8 nm. Roughness at the PbSe/Ca and Ca/Al interfaces is approximately twice as great because the NC film is granular and the calcium layer probably exists as aggregated three-dimensional (3D) islands rather than a smooth, conformal film.[3] As we show below, the roughness of these layers should be taken into account in order to achieve high-quality fits to the experimental reflectance curves.

Our optical model is based on the 2 × 2 scattering matrix formalism of Pettersson et al. that calculates the optical electric field distribution within a device stack as a function of depth and wavelength.[4−12] The model assumes isotropic and homogeneous layers separated by plane parallel interfaces. The inputs to the model include the index of refraction $n(\lambda)$, extinction coefficient $k(\lambda)$ and thickness of each layer, as well as the spectral irradiance, angle of incidence and polarization of the illumination. Surface roughness is treated by assigning a Gaussian spread to the thickness of each layer according to Lérondel et al.[13] Reflections at the air/glass interface and dispersion within the glass substrate are also included. The model yields the spectral reflectance ρ and transmittance τ of the device, the absorptance α in each layer, and the number of photons absorbed (the generation rate G) as a function of wavelength and depth in the device. At each wavelength, the average rate of photon absorption at a distance x into the device is proportional to the product of the modulus squared of the optical electric field $E(\lambda, x)$, the index of refraction $n(\lambda, x)$ and the absorption coefficient $\alpha(\lambda, x)$, divided by the photon energy $h\nu$,

$$G(\lambda, x) = \frac{c\epsilon_0 \alpha(\lambda, x) n(\lambda, x) |E(\lambda, x)|^2}{2h\nu} \quad (1)$$

where $\alpha(\lambda, x) = 4\pi k(\lambda, x)/\lambda$.

The model was parametrized with $n(\lambda)$ and $k(\lambda)$ values calculated from spectroscopic ellipsometry data of the different layers prepared on silicon or glass substrates and measured in air under a continuous flow of dry nitrogen. NC films of several thicknesses were measured to determine if the optical constants of the active layer depend on thickness. Figure 2 shows $n(\lambda)$ and $k(\lambda)$ of 80 and 185 nm thick NC films relative to the values for bulk PbSe.[14] No trends with thickness were identified. However, some scatter

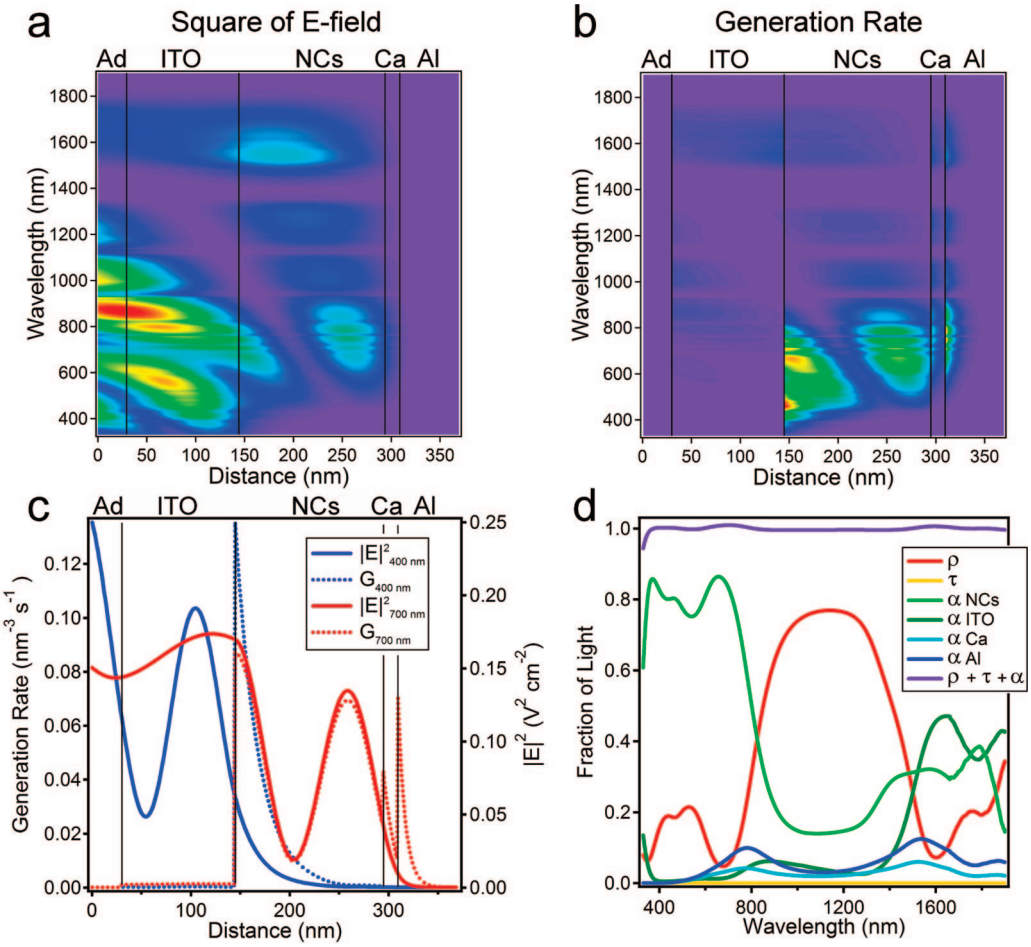

Figure 5. Model output for a device consisting of [glass/adhesion layer(30 nm)/ITO(115 nm)/NCs(150 nm)/Ca(15 nm)/Al(60 nm)] with no interfacial roughness. Light (100 mW cm^{-2} AM1.5G) is incident on the stack from the left (through the glass, which is not shown). (a) Modulus squared of the electric field (V^2 cm^{-2}). (b) The photon absorption rate (nm^{-3} s^{-1}). Photon absorption (and thus $G(\lambda, x)$) is discontinuous at the interfaces because the optical functions change at the interfaces. (c) Profiles of $|E(x)|^2$ and the generation rate for $\lambda =$ 400 and 700 nm. Note the strong interference structure of the 700 nm light. (d) Reflectance (ρ), transmittance (τ), and absorptance (α) curves of this device stack. The sum of ρ and τ with the total α is $\sim$1.

in the optical constants was found, particularly for $k(\lambda)$ in the IR wavelengths, where $k(\lambda)$ is small in magnitude and therefore difficult to determine accurately with ellipsometry. The variation in $n(\lambda)$ between the two films in Figure 2 is less than 10% across the spectrum, while the $k(\lambda)$ values vary by less than 10% from 300−1000 nm but diverge somewhat into the near-IR. The film-to-film variation in the IR $k(\lambda)$ values of the NC layers must be borne in mind when interpreting the IQE results from our model, as discussed below. The optical constants of calcium could not be determined by ellipsometry because calcium oxidizes too rapidly in air to allow reliable measurements; values from literature were used instead,[15] and checked against reflectance measurements of glass/barrier/ITO/Ca stacks to ensure that good fits were obtained. The fits for both calcium and aluminum layers on ITO are provided in Figure S2 of the Supporting Information, which also contains a file of the optical constants of each layer used in the model. The resulting optical penetration depths [$1/\alpha(\lambda)$] of the NC, ITO, Ca, and Al layers are compared in Figure 3.

The experimental and modeled reflectance curves of a series of devices of different NC film thickness are presented in Figure 4. The good fits to the experimental data suggest that the model successfully accounts for the optics of these device stacks, giving us confidence that the calculated absorptance of each layer is reasonable. Interference effects are pronounced in the reflectance of each of the devices except the stack without a NC layer. A detailed picture of the fate of light in a cell is shown in Figure 5, where $|E(\lambda, x)|^2$, $G(\lambda, x)$, ρ-τ-α, and two generation profiles are plotted for a device with a 150 nm thick NC film. The monochromatic generation profiles in Figure 5b are exponential only for $\lambda < 450$ nm. Longer wavelengths experience substantial interference within the NC film, resulting in a NC absorptance spectrum (Figure 5d) that is much different than the absorbance of the NCs in solution (Figure 1c.). Figure 6 shows the integrated generation profile of this device and several others of different thickness for 100 mW cm^{-2} AM1.5G illumination. Approximately 46% of the incident solar flux from 330−1900 nm is absorbed by the 150 nm thick NC layer; this increases to 67% for a NC layer 1200 nm thick and levels off thereafter (Figure 6b).

With a convincing model in hand, EQE and reflectance measurements can be combined to determine the IQE spectra

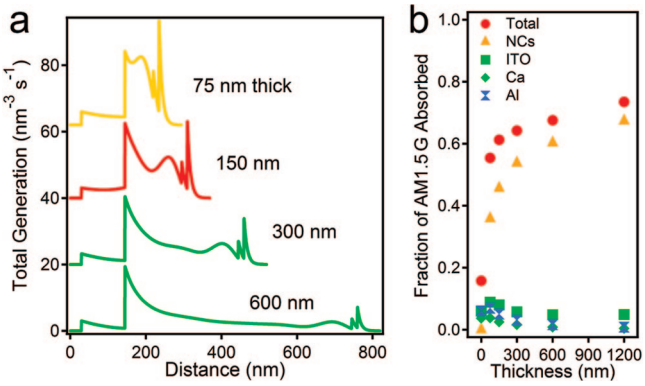

Figure 6. (a) Total generation rate ($330 \leq \lambda \leq 1900$ nm) for devices of different NC layer thickness. The device stack is identical to the geometry in Figure 5: [glass/adhesion(30 nm)/ITO(115 nm)/NCs(x nm)/Ca(15 nm)/Al(60 nm)]. The devices are illuminated with 100 mW cm^{-2} AM1.5G light from the left. Plots are offset for clarity. (b) The fraction of the incident photon flux (330−1900 nm) absorbed within each layer of the device as a function of NC layer thickness. The total photon flux in this wavelength range is 3812 photons nm^{-2} s^{-1}.

of the active layer of NC devices as a function of device thickness. IQE plots of five devices as calculated from EQE(λ)/α_{NC}(λ) are presented in Figure 7. Each device destined for EQE measurement was prepared simultaneously with its counterpart for reflectance measurement in order to ensure that the device stacks were of the same thickness. A calculated fit to each reflectance curve was used to extract α_{NC}, and the ratio of EQE over α_{NC} gave the QE spectrum of photons absorbed only within the NC layer. Figure 7 shows that the shapes of the NC absorptance spectrum and EQE spectrum of a given device are similar, confirming that the model correctly accounts for the interference effects that modulate these spectra. It is clear, particularly from the IR data of the thinnest device (60 nm), that only the NC layer contributes to the photocurrent of our cells. We see that the IQE of the two thinnest devices (60 and 125 nm) is fairly flat at 70−80 ± 7% from 350−1100 nm but decreases steadily into the infrared. Because these thin devices are thinner than the width of the depletion layer (estimated to be 100−125 nm),[1] the efficiency of light conversion is expected to be high and fairly flat across the spectrum. The abnormal IQE falloff in the infrared, seen to a degree in every device, may be explained in one of two ways. The first possibility is that the IQE falloff is an artifact caused by an overestimated $k(\lambda)$ of the NC layer in this region of the spectrum. As mentioned above, the small value of $k(\lambda)$ for $\lambda > 1200$ nm results in significant sample-to-sample scatter in $k(\lambda)$ as determined by ellipsometry. Calculations utilizing the optical constants of the 80 nm NC film rather than the 185 nm film in Figure 2 lead to much flatter IQE spectra across most of the IR without affecting the UV/visible results, but we have no reason a priori to favor the $k(\lambda)$ values of the thinner film, for which the error in the ellipsometry fit should actually be larger. We must therefore acknowledge that the IQE falloff may be a real effect.

If the IQE decline in the IR is real, it cannot be explained by trends in generation profiles with wavelength. Consider,

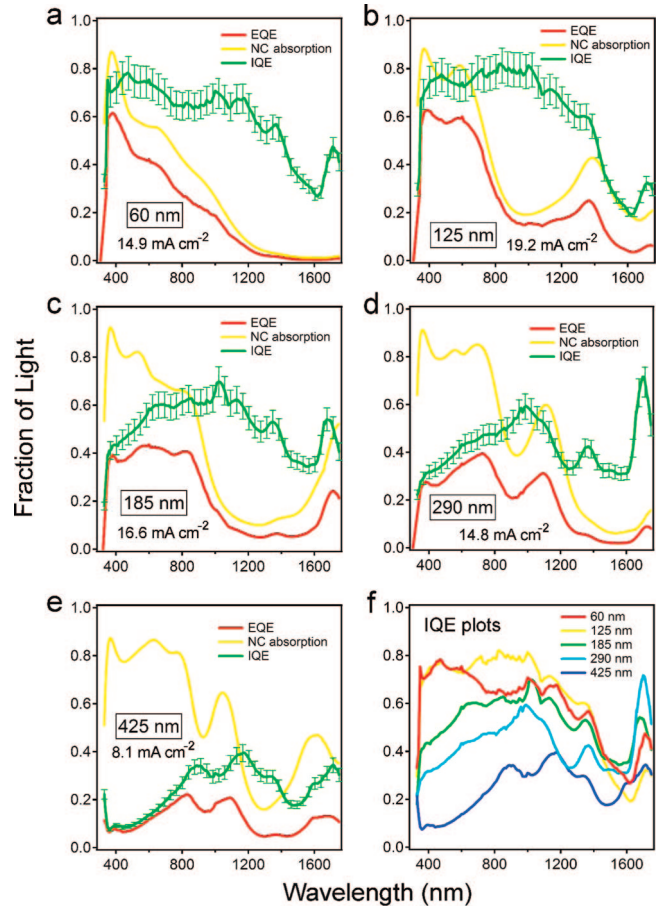

Figure 7. (a−e) Experimental EQE, modeled NC absorptance, and the resulting IQE spectra of five devices of different NC film thickness, from 60 to 425 nm. Although complete spectra (330−1750 nm) are shown, IQE data for wavelengths above 1620 nm are unreliable because of sample-to-sample differences in the position of the first excitonic transition centered at 1750−1800 nm (the first exciton redshifts from 1686 nm because of dielectric effects and inter-NC electronic coupling in the films).[2] The peak in each IQE at ~1700 nm originates from this artifact. Error bars are estimates only, assuming a 5% relative error in the quantum efficiency of the reference diode used for EQE measurements and a 5% error in the $n(\lambda)$, $k(\lambda)$ and thickness data used to extract α_{NC}. The uncertainty in the infrared (>1100 nm) is probably larger than indicated here due to the error in determining small values of $k(\lambda)$ in the ellipsometry measurements (as discussed in the text). Our modeling reduces some of this uncertainty by using a nonlinear least-squares fitting routine applied to several different samples of different thickness. The EQE data were linearly extrapolated to zero below 330 nm. The current density produced by integrating the product of the EQE of each device with the AM1.5G spectrum is shown. (f) IQE plots of the five devices. For comparison, the QE spectra of photons absorbed by the entirety of each device stack, $EQE(\lambda)/[1 - \rho(\lambda)]$, are provided in Supporting Information, Figure S4.

for instance, the 125 nm thick NC device in Figure 7b, which shows an IQE of 75% at $\lambda = 400$ nm but only 30% at $\lambda = 1500$ nm, despite the fact that a much greater proportion of the incident 1500 nm light is absorbed in the second half of the NC film, closer to the Schottky junction (31%, compared to 7% of the 400 nm light). If anything, the IQE at 1500 nm should be higher than that at 400 nm if it is determined only by the location of light absorption in the device. Similarly, the 60 nm thick NC device in Figure 7a should have a flat

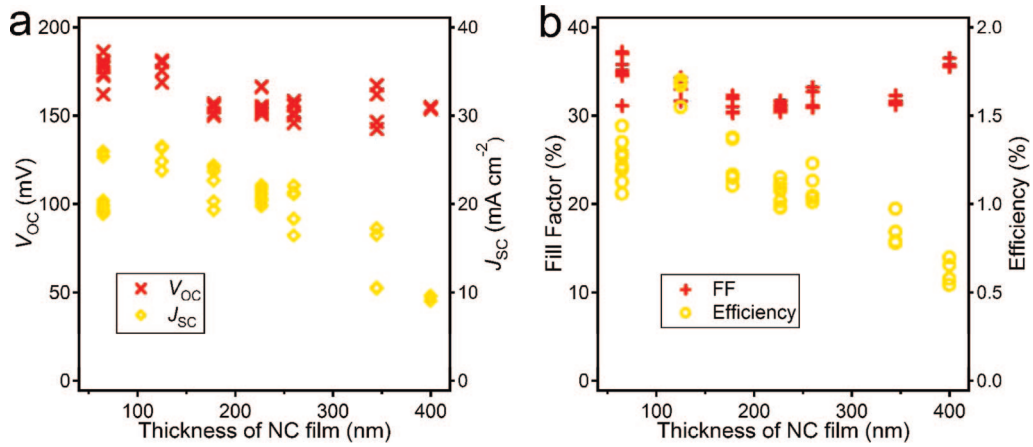

Figure 8. Trends in V_{OC}, J_{SC}, fill factor and efficiency with NC film thickness. (a) V_{OC} and J_{SC}. (b) Fill factor and efficiency. The J_{SC} values are systematically larger than the integrated EQE values in Figure 7 because (i) they are not corrected for spectral mismatch and (ii) the EQE may increase slightly with higher illumination intensity (light bias effects).[18] Possible light bias effects in these cells are the subject of ongoing study.

IQE spectrum because it is fully depleted and therefore insensitive to where light absorption occurs. The decreasing infrared IQE observed for all device thicknesses suggests that photocurrent collection is governed by the photon energy as well as the generation profile at each wavelength.

We propose that the falloff in infrared IQE may occur because lower-energy photons produce cooler excitons that have a greater tendency to recombine before escaping from their parent NC. Visible photons, on the other hand, produce relatively high-energy excitons with a greater tendency to dissociate into free carriers and delocalize throughout the NC film, thereby more efficiently contributing to photocurrent. This type of energy-dependent branching ratio for the production of excitons versus free carriers is commonly observed in conjugated polymers[15,16] and is not an unexpected feature of electronically coupled NC solids in which each NC acts as a potential energy well. However, additional work is needed to determine whether this effect is occurring in our NC devices.

As the thickness of the NC layer is increased, IQE performance becomes progressively poorer overall, especially in the blue, because the layer thickness exceeds the sum of the depletion width and diffusion length such that a dead region is established close to the ITO contact. The increasing IQE from 350−1000 nm (Figure 7c−e) is caused by the higher recombination probability of excitons created by photons absorbed closer to the ITO within this dead region. Referring to Figure 5b, we see that the fraction of light absorbed in the first half of the NC layer (nearest the ITO) decreases with increasing wavelength until $\lambda = 1000-1200$ nm. This trend is general for cells with NC layers 150−450 nm thick (Supporting Information, Figure S3) and explains the positive slope of the visible IQE of our thicker devices. In summary, the IQE of the thicker devices at $\lambda <$ 1000−1200 nm is primarily determined by where light is absorbed within each cell relative to the location of the electric field of the Schottky junction.

The data set in Figure 7 enables us to comment on the trends in solar cell performance as a function of device thickness. As expected from the EQE spectra, the short-circuit current density (J_{SC}) peaks at a NC layer thickness of about 125−150 nm and steadily decreases for thicker devices (Figure 8). The falloff in J_{SC} (and efficiency) is driven, as mentioned above, by the loss of carriers generated by blue light in the field-free region of the thicker devices, as well as the greater overall recombination in the thicker films. On the basis of the trend in J_{SC}, we estimate that the sum of the Schottky barrier depletion width and the diffusion length for electrons is approximately 150 nm in these NC films. The open-circuit voltage (V_{OC}) also decreases with thickness, but only by 30 mV, while the fill factor is flat. The V_{OC} is thought to be determined primarily by the barrier height at the NC/metal junction, and its slight decrease may reflect the greater degree of recombination occurring in the thicker devices.

We have developed an optical model for thin film NC solar cells that can calculate $E(\lambda, x)$ and determine ρ-τ-α and the carrier generation rate under arbitrary illumination. Once parametrized with the optical constants of the layers in the device stack, the model accurately reproduces our experimental reflectance curves and provides reliable estimates of light absorption in the individual ITO, NC, Ca, and Al layers. The shapes of the experimental EQE spectra agree well with those of the calculated absorptance spectra; their ratios give well-constrained IQE spectra that offer insight into the operation of these devices. We find, first of all, that interference effects must be considered in order to calculate meaningful generation profiles and IQE spectra. Generation profiles of the Beer's Law form, $G(x) = \alpha I_0 e^{-\alpha x}$, are accurate only for thicker devices at shorter wavelengths. Second, EQE and IQE values of the thinner cells reach broad maxima of 60 ± 5% and 80 ± 7%, respectively. This shows that (i) large currents can be collected from NC solids despite their relatively short diffusion lengths, as we recently demonstrated,[1] and (ii) there is no evidence of multiple exciton generation photocurrent from these EDT-treated NC devices. The absence of MEG photocurrent is consistent with recent transient absorption results indicating that the MEG ef-

ficiency is very low in EDT-treated NC films.[19] Strong inter-NC coupling caused by total removal of the original oleate ligands during treatment with EDT[2] may result in inter-NC charge-transfer processes competing with multiexciton formation, thus lowering the MEG yield. Finally, the dependence of the IQE spectra on device thickness corroborates the back-contact Schottky model recently proposed by us[1] and by Koleilat et al.[20] to explain the operation of these devices. The decrease in the infrared IQE in Figure 7 may be either an artifact or evidence that lower-energy photons tend to produce trapped excitons rather than free carriers. The optical model described here is applicable to planar thin film devices generally and will provide a powerful tool to optimize future NC solar cell designs, particularly when combined with a microscopic electrical model.

Acknowledgment. The authors thank Q. Song and B. Hughes for nanocrystal synthesis, B. To for AFM, D. Levi for assistance with ellipsometry, and D. Ginley for use of the glove boxes. M.C.B., J.M.L., and A.J.N. were supported by the Chemical Sciences, Geosciences, and Biosciences Division of the Office of Basic Energy Science of the U.S. DOE, contract DE-AC36-99-GO10337; M.L. acknowledges support from the Energy Efficiency and Renewable Energy Photovoltaics Program.

Correspondence and requests for materials should be addressed to M.L. or M.C.B.

Supporting Information Available: This material is available free of charge via the Internet at http://pubs.acs.org.

References

(1) Luther, J. M.; Law, M.; Song, Q.; Reese, M. O.; Beard, M. C.; Ellingson, R. J.; Nozik, A. J. in press.
(2) Luther, J. M.; Law, M.; Song, Q.; Perkins, C. L.; Beard, M. C.; Nozik, A. J. *ACS Nano* **2008**, *2*, 271–280.
(3) No attempt was made to confirm Ca island growth on the NC film with AFM because of the complications caused by rapid oxidation of Ca in air. However, a rough Ca layer is consistent with our modeling results. Also, see Zhu, J.; Goetsch, P.; Ruzycki, N.; Campbell, C. T. *J. Am. Chem. Soc.* **2007**, *129*, 6432–6441.
(4) Pettersson, L. A. A.; Roman, L. S.; Inganäs, O. *J. Appl. Phys.* **1999**, *86*, 487–496.
(5) Pettersson, L. A. A.; Roman, L. S.; Inganäs, O. *J. Appl. Phys.* **2001**, *89*, 5564–5569.
(6) Peumans, P.; Yakimov, A.; Forrest, S. R. *J. Appl. Phys.* **2003**, *93*, 3693–3723.
(7) Hoppe, H.; Arnold, N.; Meissner, D.; Sariciftci, N. S. *Thin Solid Films* **2004**, *451−452*, 589–592.
(8) Persson, N. K.; Arwin, H.; Inganäs, O. *J. Appl. Phys.* **2005**, *97*, 034503-
(9) O'Connor, B.; An, K. H.; Pipe, K. P.; Zhao, Y.; Shtein, M. *Appl. Phys. Lett.* **2006**, *89*, 233502.
(10) Moulé, A. J.; Bonekamp, J. B.; Meerholz, K. *J. Appl. Phys.* **2006**, *100*, 094503.
(11) Sievers, D. W.; Shrotriya, V.; Yang, Y. *J. Appl. Phys.* **2006**, *100*, 114509.
(12) Dennler, G.; Forberich, K.; Scharber, M. C.; Brabec, C. J.; Tomiš, I.; Hingerl, K.; Fromherz, T. *J. Appl. Phys.* **2007**, *102*, 054516.
(13) Lérondel, G.; Romestain, R. *Appl. Phys. Lett.* **1999**, *74*, 2740–2742.
(14) Suzuki, N.; Sawai, K.; Adachi, S. *J. Appl. Phys.* **1995**, *77*, 1249–1255.
(15) Arkhipov, V. I.; Emelianova, E. V.; Bässler, H. *Phys. Rev. Lett.* **1999**, *82*, 1321–1324.
(16) Scheblykin, I. G.; Yartsev, A.; Pullerits, T.; Gulbinas, V.; Sundström, V. *J. Phys. Chem. B* **2007**, *111*, 6303–6321.
(17) Data for 300−900 nm were taken from (a) Ramsdale, C. M.; Greenham, N. C. *J. Phys. D* **2003**, *36*, L29–L34. Data were extrapolated into the NIR using (b) Potter, M. R.; Green, G. W. *J. Phys. F: Metal Phys.* **1975**, *5*, 1426.
(18) Hohl-Ebinger, J.; Hinsch, A.; Sastrawan, R.; Warta, W.; Würfel, U. Proceedings of the 19th European Photovoltaic Solar Energy Conference, Paris, 2004.
(19) Beard, M. C.; Midgett, A.; Law, M.; Nozik, A. J. National Renewable Energy Laboratory, Golden, Colorado. Unpublished work, 2008.
(20) Koleilat, G. I.; Levina, L.; Shukla, H.; Myrskog, S. H.; Hinds, S.; Pattantyus-Abraham, A.; Sargent, E. H. *ACS Nano* **2008**, *2*, 833–840.

NL802353X